vibration

MDPI

Article

Stick–Slip Suppression in Drill String Systems Using a Novel Adaptive Sliding Mode Control Approach

Fourat Zribi [1,2], Lilia Sidhom [2] and Mohamed Gharib [1,3,*]

[1] Department of Mechanical Engineering, Texas A&M University at Qatar, Doha 23874, Qatar
[2] Laboratory of Energy Applications and Renewable Energy Efficiency (LAPER), Faculty of Sciences of Tunis, El Manar University, Tunis 1068, Tunisia
[3] Department of Engineering Technology and Industrial Distribution, Texas A&M University, College Station, TX 77843, USA
* Correspondence: mgharib@tamu.edu

Abstract: A novel control technique is presented in this paper, which is based on a first-order adaptive sliding mode that ensures convergence in a finite time without any prior information on the upper limits of the parametric uncertainties and/or external disturbances. Based on an exponent reaching law, this controller uses two dynamically adaptive control gains. Once the sliding mode is reached, the dynamic gains decrease in order to loosen the system's constraints, which guarantees minimal control effort. The proof of convergence was demonstrated according to Lyapunov's criterion. The proposed algorithm was applied to a drill string system to evaluate its performance because such systems present variable operating conditions caused by, for example, the type of rock. The effectiveness of the proposed controller was evaluated by conducting a comparative study that involved comparing it against a commonly used sliding mode controller, as well as other recent adaptive sliding mode control techniques. The different mathematical performance measures included energy consumption. The proposed algorithm had the best performance measures with the lowest energy consumption and it was able to significantly improve the functioning of the drill string system. The results indicated that the proposed controller had 20% less chattering than the classic SM controller. Finally, the proposed controller was the most robust to uncertainties in system parameters and external disturbances, thus demonstrating the auto-adjustable features of the controller.

Keywords: first-order sliding mode; dynamic gains controller; comparative study; parametric uncertainties; external perturbation; drill string application

check for updates

Citation: Zribi, F.; Sidhom, L.; Gharib, M. Stick–Slip Suppression in Drill String Systems Using a Novel Adaptive Sliding Mode Control Approach. *Vibration* **2024**, *7*, 479–502. https://doi.org/10.3390/vibration7020026

Academic Editor: Aleksandar Pavic

Received: 22 March 2024
Revised: 3 May 2024
Accepted: 3 May 2024
Published: 23 May 2024

Copyright: © 2024 by the authors. Licensee MDPI, Basel, Switzerland. This article is an open access article distributed under the terms and conditions of the Creative Commons Attribution (CC BY) license (https://creativecommons.org/licenses/by/4.0/).

1. Introduction

Sliding mode controllers (SMCs) are advanced control methods that are widely used in uncertain systems with external disturbances that satisfy a matching condition [1]. As a variable structure control method, SMCs utilize a discontinuous control law that enables the closed-loop system to converge in a finite time. SMCs have gained significant attention from researchers because of their robustness to parameter variations and external perturbations [2,3], which makes them an attractive scheme for controlling different kinds of systems [4]. It has been used in different research fields such as power electronics [5], power systems [6], electromechanical systems [3,7], biological economics [8], the space industry [9], robotics [10], and drilling systems [11,12]. Despite the successful use of SMCs, it has some drawbacks [2]. In fact, prior knowledge of the upper bounds of the uncertainties and external disturbances is necessary for designing a sliding mode (SM) controller. These upper bounds are poorly known; generally, their values are overestimated in order to compensate for their effects. However, overestimation of these bounds can lead to excessive gains. In contrast, frequent switching of the control gain can lead to the chattering phenomenon, especially for first-order SMCs because of the discontinuous switching law. This harmful phenomenon is undesirable because it causes energy losses and

damage to the system's components, and reduces its lifetime. Various methods have been studied to address the issue of chattering. Several artificial intelligence-based techniques have been applied to the SM technique [13,14], such as fuzzy rule-based algorithms that result in smooth dynamics when the system is near the switching region. Other techniques include the use of high-order SM controllers to reduce chattering. The authors of [15] proposed a second-order SMC for the control of robot manipulators that showed good tracking performance with minimal chattering. However, prior awareness of the upper limits of the uncertainties was necessary for implementing the proposed controller and it also needed information about the successive derivatives of the sliding surface. In [16], the authors implemented a super-twisting algorithm for controlling a four-rotor helicopter. The studied control algorithm managed to reduce the chattering phenomenon taking into account modelling imprecisions and external factors. The authors in [17] combined the fractional-order nonsingular SMC, the super-twisting SMC, and a double-loop fuzzy neural network algorithm for controlling a micro-gyroscope with unknown uncertainties. The proposed controller had the advantage of the fractional order controller, which improved the flexibility of the control and the super-twisting algorithm, and, thus, effectively solved the chattering problem. In [18], the authors presented a sliding mode control (SMC) method that utilizes a double-hidden-layer recurrent neural network with fuzzy logic to regulate a single-phase active power filter. The proposed algorithm guaranteed the control of the active power filter with great precision. However, the definition of the fuzzy rules was very complex, and the controller's performance depended directly on the number of fuzzy rules implemented. An experimental investigation of a recurrent neural network fractional-order SMC applied on an active power filter was provided in [19]. The experimental outcomes confirmed the efficiency of the proposed control algorithm regarding the robustness and compensation performance compared with the standard neural SMC. However, the main disadvantage of the proposed algorithm was that it required much more data than traditional machine learning algorithms. With the exception of the super-twisting algorithm, higher-order sliding mode (SM) algorithms are only suitable for systems with a relative degree above one. One way to effectively reduce chattering and eliminate the need for a priori knowledge of uncertainty bounds is by defining dynamic SM controller gains with respect to the sliding surface.

Different adaptive SMC schemes have been proposed in the literature. To address the issue of chattering, the authors in [20] developed an adaptive SMC strategy for controlling a micro-AUV in the presence of water currents and parametric uncertainties. In [21], the authors designed an embedded flight controller based on the adaptive SM technique. Both of these previous studies investigated similar algorithms for adaptive gains based on index-reaching laws. Depending on the sliding surface, the dynamic gain was defined either by a constant that set the minimal value of the gain or by an expression containing the sign function of the sliding variable multiplied by the rate of adaptation. Both control strategies demonstrated the ability to effectively track the desired velocity within an acceptable time frame. Nevertheless, the proposed controllers lacked experimental validation to confirm their efficacy. The authors of [22] proposed an adaptive form of the controller proposed in [18]. The proposed adaptive sliding mode control demonstrated superior compensation performance and tracking accuracy when compared to the basic SMC. The authors introduced two first-order adaptive sliding mode controllers that employ constant reaching laws. The gain dynamics of the first controller included a low-pass filter to obtain the average of the sign function when the sliding region had been reached, and a constant reaching law to ensure convergence to the SM. If this filter is not properly adjusted, it may distort the signal, for example, through loss of information by attenuating magnitude. However, a phase shift is inevitable with a low-pass filter. To avoid the use of such a filter, the second control law is defined by a dynamic gain involving the sliding surface's absolute value. The authors of [23] used an adaptive gain similar to [1]. However, the discontinuous control law included the sliding surface term without any functions, including the sign function. The authors of [24] proposed a second-order SM controller in which the gain

gradually increased until the SM had been reached. However, the gain of the proposed algorithm never decreases, which can result in an overestimation of the gain and more chattering. The authors of [25] proposed a higher-order adaptive SM controller. This approach featured a unique dual-layer structure that relied on the application of equivalent injection principles and necessitated the existence of the first and second derivatives of the uncertainty. In [26], the authors investigated an adaptive SMC based on an exponential-reaching law. A simple adaptation scheme based on a single adaptive gain was used as an adaptive law for the controller gain. The controller showed great robustness to parameter uncertainties and external disturbances. Yet, a considerable amount of fluctuation remained at the bit velocity when applied with measurement noise.

It is important to note that inadequate estimation of either the uncertainties or the external disturbances results in more chattering and minimizes the robustness of the controller. For complex systems, such as drill strings, the uncertainties and external perturbations are significantly hard to predict since they are directly related to several factors such as the operating mode and condition. However, adapting the SM controller gains makes it possible to ensure a SM that is independent of these upper bounds. In this paper, a new adaptive SMC design is proposed to tackle the uncertainties and disturbances in a system that needs to be controlled, without prior knowledge. Various simulations were carried out to test its ability to reduce torsional vibrations while maintaining good tracking performance, and also to test its robustness regarding some parametric uncertainties. We also evaluated its performance under different operating conditions and external perturbations. The novel adaptation law proposed in this paper is distinguished by the utilization of two dynamically adapted gains that are inversely proportional to the sliding variables. The new adaptive scheme can make the system converge rapidly in a finite time and can reduce the chattering phenomenon in the traditional SMC. The proposed reaching law guarantees that the control constraints on the system will be minimal since both gains decrease once the SM has been reached. However, the proposed controller can be effectively implemented, ensuring good performance even in the presence of external perturbations and across diverse operating conditions.

This paper makes the following contributions to the literature:

1. Design of a novel adaptive SMC with first-order dynamics, without requiring advance information of the uncertainties and external perturbations' upper bounds, thus significantly decreasing the chattering phenomenon while enhancing the controller component's lifespan;
2. Application of the proposed controller to a drill string system under various operating regimes.
3. Comparative study of the first-order SM adaptive and proposed controllers. It includes a data analysis and a discussion to evaluate the performance of the proposed controller in comparison to the ones presented in the literature.

The structure of this paper can be summarized as follows. Section 2 provides the design strategy of the proposed controller along with a demonstration of its finite-time convergence via Lyapunov's direct method. Section 3 describes the application of the proposed controller to a drill string system. In Section 4, the simulation results and an evaluation of the closed-loop system's performance are discussed. Finally, the conclusions are presented in Section 5.

2. Control Strategy

This section provides a detailed description of the design process for the proposed adaptive sliding mode controller. The goal of this paper was to design an adaptive SMC with an interesting exponent-based convergence law. The novel scheme ensures dynamically adaptive gains, resulting in fast and precise convergence.

2.1. Problem Statement

Let us suppose a nonlinear system that includes external disturbances, which can be presented as follows:

$$\begin{cases} \dot{\mathbf{x}}(t) & = A\mathbf{x}(t) + B\,u(t) + d(t) \\ \mathbf{y}(t) & = C\,\mathbf{x}(t) \end{cases} \tag{1}$$

where A and B are input matrices, C is defined to have $y(t) \in \Re$. $u(t) \in \Re$ is the control input, $x(t) \in \Re^{(n)}$ is the state vector, and $d(t)$ presents the bounded external perturbations satisfying $||d(t)|| < L$ where $L > 0$ is the upper limit of the disturbance. Note that the system mentioned in Equation (1) has a relative degree that is equal to one. The main target of the controller is to force the output of the system $y(t)$ to follow a desired value $y_d(t)$, which means that the error presenting the deviation from the desired trajectory can be written as follows:

$$e(t) = \mathbf{y}(t) - \mathbf{y}_d(t) \tag{2}$$

If $e(t)$ reaches a small value (i.e., $e \to 0$), the controller's objective is achieved. The sliding surface term can be presented as follows:

$$s(t) = \dot{e}(t) + \lambda e(t) \tag{3}$$

Substitution of Equations (1) and (2) into Equation (3) results in:

$$\begin{aligned} s(t) = CA\mathbf{x}(t) + Cd(t) + \lambda(\mathbf{y}(t) - \mathbf{y}_d(t)) \\ - \dot{\mathbf{y}}_d(t) + CB\,u(t) \end{aligned} \tag{4}$$

As previously stated, let us suppose that the sliding variable s has a relative degree of 1 with respect to the control input. The expression for the first derivative of the sliding surface described in Equation (4) can be expressed as follows:

$$\dot{s} = \psi(x(t)) + \Gamma(x(t))u(t) \tag{5}$$

It is assumed that the functions $\psi(x(t))$ and $\gamma(x(t))$, which belong to the set '$\Re$', are uncertain and can be expressed as follows:

$$\begin{cases} \psi(x(t)) = \psi_{nom}(x(t)) + \Delta\psi(x(t)) \\ \Gamma(x(t)) = \Gamma_{nom}(x(t)) + \Delta\Gamma(x(t)) \end{cases} \tag{6}$$

where the nominal known functions are $\psi_{nom}(x(t))$ and $\Gamma(x(t))$ and $\Delta\psi(x(t))$ and $\Delta\Gamma(x(t))$ present the uncertainties terms. We also assume that $\psi_{nom}(x(t))$ and $\Gamma(x(t))$ are limited in the following manner:

$$\begin{cases} |\ \psi(x(t))\ | \leq \psi_M \\ 0 < \Gamma_m \leq \Gamma(x(t)) \leq \Gamma_M \end{cases} \tag{7}$$

where ψ_M, Γ_m and Γ_M are the bounds of $\psi(x(t))$ and $\Gamma(x(t))$, respectively. These bounds are supposed to exist but are not known. According to [25], the sliding surfaces for a given system must be defined as the following set with $\rho > 0$ being the upper bound of s:

$$s = \{x \in \chi, |s(x,t)| < \rho\} \tag{8}$$

2.2. Design of the Proposed Controller

The control law must be chosen so that the sliding surface, s, approaches zero in finite time. The control input u is expressed as follows:

$$u = u_{eq} + u_{disc} \tag{9}$$

The equivalent control u_{eq} can be obtained by solving $\dot{s} = 0$, while u_{disc} represents the controller's discontinuous component. The adaptive SMC proposed in this study can be expressed as follows:

$$u_{disc} = -\hat{k_1}(t)|s|^{1/2} sign(s) - \hat{k_2}(t)s \tag{10}$$

where

$$\hat{k_2}(t) = a\,\hat{k_1}(t) \tag{11}$$

The two equations defining the dynamic gains of the controller depend on the switching conditions given below:

$$\dot{\hat{k_1}}(t) = \begin{cases} \mu_1 |s|^b sign(|s| - \delta) & \text{if} \quad \hat{k_1}(t) > \alpha \\ \mu_2 & \text{if} \quad \hat{k_1}(t) \leq \alpha \end{cases} \tag{12}$$

The positive constants b, δ, μ_1, and μ_2, and the small positive constants $\alpha << 1$ and $a << 1$ are used in the following equations. At the initial time, $t = 0$, the value of $\hat{k_1}(0)$ should be greater than α to ensure that $\hat{k_1}(t)$ remains positive.

The dynamics of the gains ensure that the adaptive gains decrease once the SM has been reached. The control law described by the system of Equation (12) imposes few constraints on the controlled system. A general diagram of the proposed control law is shown in Figure 1.

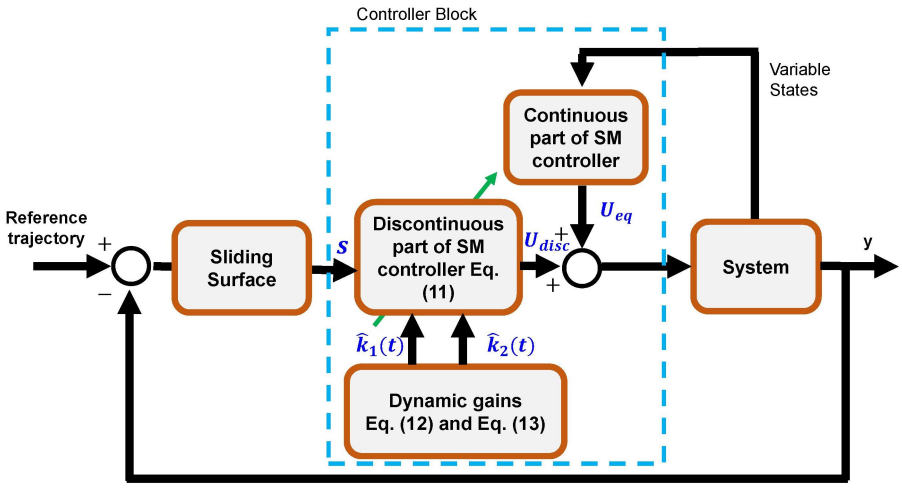


Figure 1. Overall architecture of the proposed control scheme.

Remark 1. *In the work of [26], the authors investigated an adaptive SMC based on an exponential-reaching law. A simple adaptation scheme based on a single adaptive gain was used as an adaptive law for the controller gain. The controller showed great robustness to parameter uncertainties and external disturbances. Yet, a considerable amount of fluctuation remained at the bit velocity when applied with measurement noise. The proposed control schedule in this paper includes a real-time update of both gains (k_1, k_2) of $u_d$isc. Therefore, it proposes an adaptive switching control based on the exponent reaching law. The adaptive update of the controller gains allows the controller to maintain good performance even when there are external disturbances or uncertainties in the system's parameters. This update also eliminates the need to reset the controller gains every time the operating conditions change. In this paper, the use of the absolute value of the sliding variable in the adaptive behavior, which was added to the classic scheme, improves the controller performance even for one operating condition without considering any perturbations/uncertainties. Compared to the work in [26], both adaptive gains in the convergence region increase quickly to a large value to counteract any disturbances. Then, the dynamic gains decrease until small values at the sliding region. Hence, it is possible to further reduce the problem related to the chattering phenomenon.*

Proof of a General Convergence

This section employs Lyapunov's direct method to prove the convergence of the closed-loop system.

Lemma 1. *The proposed controller, given by Equation (11), and implemented on system (1) with dynamic gains defined by Equations (12) and (13), ensures that the gain $\hat{k_1}(t)$ is upper-bounded by a positive constant $\bar{k_1}$, as demonstrated below.*

$$0 < \hat{k_1}(t) \leq \bar{k_1}, \forall t > 0 \tag{13}$$

Proof. If we take the first derivative of the sliding surface presented in Equation (5) and the controller described by Equations (11)–(13), the candidate Lyapunov function is chosen to be [26]:

$$V(t) = \frac{1}{2}s^2 + \frac{1}{2\gamma}(\hat{k_1}(t) - \bar{k_1})^2 \tag{14}$$

The derivative along the trajectory of the function $V(t)$ is given by the following:

$$\dot{V(t)} = s\dot{s} + \frac{1}{\gamma}(\hat{k_1}(t) - \bar{k_1})\mu_1|s|^b sign(|s| - \delta) \tag{15}$$

Substituting the expression of s, as defined in Equations (6) and (15), can be rewritten as follows:

$$\begin{aligned} \dot{V(t)} = s\psi(x(t)) + s\Gamma(x(t))u(t) \\ + \frac{1}{\gamma}(\hat{k_1}(t) - \bar{k_1})\mu_1 \mid s \mid^b sign(\mid s \mid -\delta) \end{aligned} \tag{16}$$

Equation (11) can now be substituted into Equation (16), yielding the following:

$$\begin{aligned} \dot{V(t)} = s\psi(x(t)) + s\Gamma(x(t))(-\hat{k_1}(t) \mid s \mid^{1/2} sign(s) - a\hat{k_1}(t)s) \\ + \frac{1}{\gamma}(\hat{k_1}(t) - \bar{k_1})\mu_1 \mid s \mid^b sign(\mid s \mid -\delta) \end{aligned} \tag{17}$$

$$\begin{aligned} \dot{V(t)} = s\psi(x(t)) - s\Gamma(x(t))\hat{k_1}(t) \mid s \mid^{1/2} sign(s) - a\Gamma\hat{k_1}(t)s^2 \\ + \frac{1}{\gamma}(\hat{k_1}(t) - \bar{k_1})\mu_1 \mid s \mid^b sign(\mid s \mid -\delta) \end{aligned} \tag{18}$$

$$\begin{aligned} \dot{V(t)} \leq \mid s \mid \psi_M - \mid s \mid \Gamma_m\hat{k_1}(t) \mid s \mid^{1/2} - a\Gamma_M\hat{k_1}(t) \mid s \mid^2 \\ + \frac{1}{\gamma}(\hat{k_1}(t) - \bar{k_1})\mu_1 \mid s \mid^b sign(\mid s \mid -\delta) \end{aligned} \tag{19}$$

Adding and substituting the term $\Gamma_m\bar{k_1}(|s|^{1/2} - a|s|)$ gives the following:

$$\begin{aligned} \dot{V(t)} \leq \mid s \mid \psi_M - \mid s \mid \Gamma_m\hat{k_1}(t)(\mid s \mid^{1/2} - a \mid s \mid) \\ + \frac{1}{\gamma}(\hat{k_1}(t) - \bar{k_1})\mu_1 \mid s \mid^b sign(\mid s \mid -\delta) \\ + \mid s \mid \Gamma_M\bar{k_1}(\mid s \mid^{1/2} - a \mid s \mid) - \mid s \mid \Gamma_m\bar{k_1}(\mid s \mid^{1/2} - a \mid s \mid) \end{aligned} \tag{20}$$

After simplification, this gives the following:

$$\begin{aligned} \dot{V(t)} \leq & \mid s \mid [\psi_M - \Gamma_m \bar{k_1}(\mid s \mid^{1/2} - a \mid s \mid)] \\ & + (\hat{k_1}(t) - \bar{k_1})[- \mid s \mid \Gamma_m \hat{k_1}(t)(\mid s \mid^{1/2} - a \mid s \mid) \\ & + \frac{1}{\gamma}\mu_1 \mid s \mid^b sign(\mid s \mid - \delta)] \end{aligned} \tag{21}$$

Let us define a positive constant β. In this case, we have the following:

$$\begin{aligned} \dot{V(t)} \leq & \mid s \mid [\psi_M - \Gamma_m \bar{k_1}(\mid s \mid^{1/2} - a \mid s \mid)] \\ & + (\hat{k_1}(t) - \bar{k_1})[- \mid s \mid \Gamma_m \hat{k_1}(t)(\mid s \mid^{1/2} - a \mid s \mid) \\ & + \frac{1}{\gamma}\mu_1 \mid s \mid^b sign(\mid s \mid - \delta)] \\ & + \beta \mid \hat{k_1}(t) - \bar{k_1} \mid - \beta \mid \hat{k_1}(t) - \bar{k_1} \mid \end{aligned} \tag{22}$$

Therefore,

$$\begin{aligned} \dot{V(t)} \leq & - \mid s \mid (-\psi_M + \Gamma_m \bar{k_1}(\mid s \mid^{1/2} - a \mid s \mid)) \\ & - \beta \mid \hat{k_1}(t) - \bar{k_1} \mid - \mid \hat{k_1}(t) \\ & - \bar{k_1} \mid s \mid^{3/2} (\Gamma_m \hat{k_1}(t)(1 - a \mid s \mid^{1/2})) \\ & - \mid \hat{k_1}(t) - \bar{k_1} \mid (\frac{1}{\gamma}\mu_1 \mid s \mid^b sign(\mid s \mid - \delta) + \beta) \end{aligned} \tag{23}$$

If the following two conditions are satisfied, then the derivative of the Lyapunov function $V(t)$ is negative, as follows:

$$\begin{cases} 1 - a|s|^{1/2} & > 0 \\ -\frac{1}{\gamma}\mu_1 sign(|s| - \delta) + \beta & > 0 \end{cases} \tag{24}$$

The first assumption, $a < 1/|s|^{1/2}$, is a direct consequence of the selected value for the constant a. As for the second inequality in Equation (24), two scenarios can be examined:

i For the case $|s| > \delta$, $\dot{V(t)}$ is negative-definite if $\mu_1 > \gamma\beta$.

ii For the case $|s| \leq \delta$, $\dot{V(t)}$ is negative-definite if $\mu_1 > -\gamma\beta$

Thus, the condition can be written as follows:

$$\mu_1 > sign(\gamma\beta) \mid \gamma\beta \mid \tag{25}$$

where μ_1 and μ_2 are the main parameters of the proposed controller. Tuning them is carried out as follows: To ensure that $\hat{k_1}(t)$ stays positive, it is important to choose a small value for μ_1, such that the initial value of the proposed gain at $t = 0$, $\hat{k_1}(0)$, is greater than α. A small value of μ_2 must be chosen, as this represents the value of the dynamic gain when the system stabilizes at the sliding region. The selection of the control parameters was done through a trial-and-error process to achieve a balance between the rate of convergence and the magnitude of chattering in the system. Moreover, a small value of b must be chosen to reduce the instant overshoot caused by the gain dynamics. □

3. Drill String Application

A drill string system is composed of various components including a rotary table, drill pipes, drill collars, and a drill bit (see Figure 2). The rotary table generates the driving torque, which is then transmitted through the drill pipes to the drill bit for rock-cutting purposes [27]. To understand the structure of a drill string system, it can be divided into three parts: the surface, middle, and bottom [12]. The surface part includes the rotary table

that is controlled by a regulator to maintain precise and robust drilling speed. The middle section contains the drill collars and drill pipes, which can span over several hundred meters to several kilometers. The bottom section consists of the drill bit that is tasked with overcoming the complicated and nonlinear bit-rock interaction, which can sometimes involve time delays.

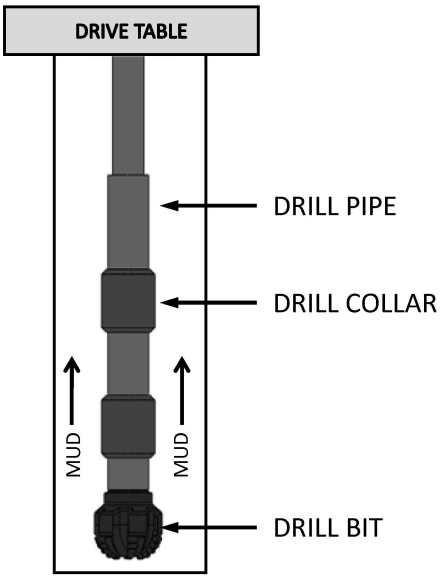


Figure 2. Schematic for the main parts of a drill string.

The rotary motion generated by the rotary table is transmitted to the drill bit through the drill string. In addition to transmitting the rotary motion, drill strings also provide the necessary weight on bit (WOB), which aids in the drilling process [28]. The system's interaction with the borehole results in various unwanted oscillations, including the stick–slip phenomenon, which is a severe form of torsional vibration that causes the drill string to stop rotating and then periodically rotate freely [29]. The main cause of this particular vibration is the highly nonlinear torque applied on the bit. This nonuniform rotation can reduce the drilling efficiency or even damage the drill string components [27]. Moreover, drill strings' parameters vary depending on the operating modes and conditions [30]. For example, it is very challenging to know the correct stiffness and damping of the drill pipes. Moreover, the WOB varies, depending on the type of rock being cut. This always makes the drill string system susceptible to external perturbations [12]. The objective of this study is to evaluate and confirm the effectiveness of the controller in eliminating the stick–slip occurrence, regardless of any external disturbances or uncertainties in the system's parameters.

3.1. Mathematical Model of the Drill String

There are various modeling techniques available to simulate the behavior of a drill string system numerically, such as those discussed in [31,32]. For pure torsional studies in particular, lumped parameter modeling has been widely used in the literature to assess stick–slip behavior [33,34]. In this study, a model with four degrees of freedom (4DOF) has been considered that includes the four subsystems described in Figure 2 [35]. The model used in this study is based on three main assumptions: (i) Only torsional vibrations are taken into account, (ii) the drill string is assumed to be vertical, and (iii) all drill pipes have the same inertia.

The dynamics of the torsional vibrations are described by the following equation [35]:

$$\begin{aligned} &J_{dt}\ddot{\varphi}_{dt} + c_{dt}\dot{\varphi}_{dt} + c_{pi}(\dot{\varphi}_{dt} - \dot{\varphi}_{pi}) + k_{pi}(\varphi_{dt} - \varphi_{pi}) = u \\ &J_{pi}\ddot{\varphi}_{pi} + c_{pi}(\dot{\varphi}_{pi} - \dot{\varphi}_{dt}) + c_{co}(\dot{\varphi}_{pi} - \dot{\varphi}_{co}) \\ &\qquad + k_{pi}(\varphi_{pi} - \varphi_{dt}) + k_{co}(\psi_{pi} - \psi_{co}) = 0 \\ &J_{co}\ddot{\varphi}_{co} + c_{co}(\dot{\varphi}_{co} - \dot{\varphi_{pi}}) + c_{bi}(\dot{\varphi}_{co} - \dot{\varphi}_{bi}) \\ &\qquad + k_{co}(\varphi_{co} - \varphi_{pi}) + k_{b}(\varphi_{co} - \varphi_{bi}) = 0 \\ &J_{bi}\ddot{\varphi}_{bi} + c_{bit}\dot{\varphi}_{bi} + c_{bi}(\dot{\varphi}_{bi} - \dot{\varphi}_{co}) \\ &\qquad + k_{bi}(\varphi_{bi} - \varphi_{co}) + T_{bit} = 0 \end{aligned} \tag{26}$$

where J_{dt}, J_{pi}, J_{co}, and J_{bi} are the moments of inertia of the top drive, drill pipes, drill collars, and drill bit; φ_{dt}, φ_{pi}, φ_{co}, and φ_{bi} are the angular positions of the top drive, drill pipes, drill collars, and drill bit; k_{pi}, k_{co}, and k_{bi} are the torsional stiffness of the drill pipes, drill collars, and drill bit; and c_{pi}, c_{co}, and c_{bi} represent the torsional damping of the drill pipes, drill collars, and drill bits. We can now define a state vector $x(t)$ as follows:

$$\begin{aligned} \mathbf{x}(t) &= (\dot{\varphi}_{dt}, \varphi_{dt} - \varphi_{pi}, \dot{\varphi}_{pi}, \varphi_{pi} - \varphi_{co}, \dot{\varphi}_{co}, \varphi_{co} - \varphi_{b}, \dot{\varphi}_{bi})^T \\ \mathbf{x}(t) &= (x_1, x_2, x_3, x_4, x_5, x_6, x_7)^T \end{aligned} \tag{27}$$

Using Equation (27), the system can be written in the following form [34]:

$$\begin{aligned} \dot{x_1} &= \frac{1}{J_{dt}}[-(c_{dt} + c_{pi})x_1 - k_{pi}x_2 + c_{pi}x_3 + u] \\ \dot{x_2} &= x_1 - x_3 \\ \dot{x_3} &= \frac{1}{J_{pi}}[c_{pi}x_1 + k_{pi}x_2 - (c_{pi} + c_{co}x_3) - k_{co}x_4 + c_{co}x_5] \\ \dot{x_4} &= x_3 - x_5 \\ \dot{x_5} &= \frac{1}{J_{co}}[c_{co}x_3 + k_{co}x_4 - (c_{co} + c_{bi})x_5 - k_{bi}x_6 + c_{bi}x_7] \\ \dot{x_6} &= x_5 - x_7 \\ \dot{x_7} &= \frac{1}{J_{bi}}[c_{bi}x_5 + k_{bi}x_6 - (c_{bi} + c_{bit})x_7 - T_{bit}(x(t))] \end{aligned} \tag{28}$$

The system presented in Equation (28) can be expressed in state space form as follows [34]:

$$\begin{cases} \dot{\mathbf{x}}(t) & = A(\mathbf{x}(t)) + Bu(t) + DT_{bit}(x(t)) \\ \mathbf{y} & = C\,\mathbf{x}(t) \end{cases}$$

Here, the matrices A, B, C, and D have dimensions of 7×7, 7×1, 1×7, and 7×1, respectively. The matrices can be expressed as follows:

$$A = \begin{bmatrix} \frac{-(c_{dt}+c_{pi})}{J_{dt}} & \frac{-k_{pi}}{J_{dt}} & \frac{c_{pi}}{J_{dt}} & 0 & 0 & 0 & 0 \\ 1 & 0 & -1 & 0 & 0 & 0 & 0 \\ \frac{c_{pi}}{J_{pi}} & \frac{k_{pi}}{J_{pi}} & \frac{-(c_{pi}+c_{co})}{J_{pi}} & \frac{-k_{co}}{J_{pi}} & \frac{c_{co}}{J_{pi}} & 0 & 0 \\ 0 & 0 & 1 & 0 & -1 & 0 & 0 \\ 0 & 0 & \frac{c_{co}}{J_{co}} & \frac{k_{co}}{J_{co}} & \frac{-(c_{co}+c_{bi})}{J_{co}} & \frac{-k_{bi}}{J_{co}} & \frac{c_{bi}}{J_{co}} \\ 0 & 0 & 0 & 0 & 1 & 0 & -1 \\ 0 & 0 & 0 & 0 & \frac{c_{bi}}{J_{bi}} & \frac{k_{bi}}{J_{bi}} & \frac{-(c_{bi}+c_{bit})}{J_{bi}} \end{bmatrix} \tag{29}$$

$$B = \begin{bmatrix} \frac{1}{J_{dt}} & 0 & 0 & 0 & 0 & 0 & 0 \end{bmatrix}^{\mathsf{T}}$$

$$D = \begin{bmatrix} 0 & 0 & 0 & 0 & 0 & 0 & \frac{-1}{J_{bi}} \end{bmatrix}^{\mathsf{T}}$$

$$C = \begin{bmatrix} 1 & 0 & 0 & 0 & 0 & 0 \end{bmatrix}$$

The torque on the bit must accurately reproduce the reaction of the borehole to the bit. The well-known models of Stribeck and Karnopp [36,37] are generally used for presenting bit–rock interactions. Both models have shown good results, but Karnopp's model has

an advantage in reproducing friction at the bit level due to its continuity at zero velocity, unlike Stribeck's friction model. The Karnopp's friction model can be expressed as follows:

$$T_{bit} = \begin{cases} T & \text{if } \mid \dot{\varphi_{bi}} \mid \leq \Delta w \quad , \mid T \mid \leq T_a \\ T_a sign(\dot{\varphi_{bi}}) & \text{if } \mid \dot{\varphi_{bi}} \mid \leq \Delta w \quad , \mid T \mid > T_a \\ [T_0 + (T_a - T_0)e^{-\xi \mid \dot{\varphi_{bi}} - \Delta w \mid}] sign(\dot{\varphi_{bi}}) & \text{if } \mid \dot{\varphi_{bi}} \mid > \Delta w \end{cases} \tag{30}$$

The maximum friction torque is denoted as $T_a = \mu_a \, WOB \, R$, and the sliding friction torque is represented by $T_0 = \mu_0 \, WOB \, R$. The parameter Δw is used as a threshold value between static and sliding friction, while ξ denotes the rate of decline in friction torque.

In the field, drill strings are generally driven by motors with a nominal velocity (vm) that can reach 1500 RPM. However, the maximal velocity of the drill bit (vb) is generally limited to 200 RPM; $n = vb/vm = 0.13 << 1$. We can conclude that the actuator's dynamics do not significantly interfere with the drill string's dynamics. In many systems, disturbances and uncertainness can significantly reduce the controller's performance. However, the SM technique has proven to be one of the most robust control techniques because it can estimate parameter variations and external disturbances that satisfy a matching condition (the disturbances are applied to the system through the same channels as the input signals, without affecting the order of the system). For the drill string system under study, the disturbances under investigation are those that act directly on the axial motion of the drill string (variation of the WOB) and directly affect the control input. It should be noted that in cases where disturbances cannot be calculated directly, they can be estimated based on the available measurements. However, a suitable control strategy needs to be developed either using these estimations or based on the measurements of the sensors to effectively counteract the perturbations.

3.2. Proof of Closed Loop Stability

The primary goal of the proposed control strategy is to regulate the bit velocity. To accomplish this, a sliding function is defined as per [37]:

$$s = (x_1 - x_d) + \lambda \int_0^t (x_1 - x_d)dt + \lambda \int_0^t (x_1 - x_7)dt \tag{31}$$

In the proposed control strategy, the desired drill string velocity is denoted by $x_d(t)$. As the system reaches the sliding region $s = 0$, it reaches the desired equilibrium point where the bit velocity approaches the desired velocity. The first-order derivative of the variable defined in the above equation can be given as follows:

$$\dot{s} = \dot{x_1} + \lambda(x_1 - x_d) + \lambda(x_1 - x_7) \tag{32}$$

Replacing $\dot{x_1}$ in the previous equation results in the following equation:

$$\dot{s} = (1/J_{dt})[u - (c_{dt} + c_{pi})x_1 - k_{pi}x_2 + c_{pi}x_3] + \lambda(x_1 - x_d) + \lambda(x_1 - x_7) \tag{33}$$

In our case, $\Gamma(x(t))$ is a positive constant defined as follows:

$$\Gamma(x(t)) = 1/J_{dt} \tag{34}$$

For this particular case, $\Gamma(x(t))$ is restricted to a single constant value, and the function $\psi(x(t))$ can be expressed as follows:

$$\psi(x(t)) = -1/J_{dt}[(c_{dt} + c_{pi})x_1 - k_{pi}x_2 + c_{pi}x_3] + \lambda(x_1 - x_d) + \lambda(x_1 - x_7) \tag{35}$$

The values of c_{dt}, c_{pi}, and k_{pi} are uncertain and can be expressed as follows:

$$\begin{cases} c_{dt} = c_{dt_{nom}} + \triangle c_{dt} \\ c_{pi} = c_{pi_{nom}} + \triangle c_{pi} \\ k_{pi} = k_{pi_{nom}} + \triangle k_{pi} \end{cases} \tag{36}$$

It is also assumed that c_{dt}, c_{pi}, and k_{pi} are bounded as follows:

$$\begin{cases} c_{dt} \leq c_{dt_M} \\ c_{pi} \leq c_{pi_M} \\ k_{pi} \leq k_{pi_M} \end{cases} \tag{37}$$

The parameters c_{dt_M}, c_{pi_M}, and k_{pi_M} represent the upper limits of c_{dt}, c_{pi}, and k_{pi}, respectively. Although these upper limits exist, their values are unknown. As a result, we can derive the following inequality:

$$\begin{aligned} \psi(x(t)) \leq \psi_{ma} = &-1/J_{dt}[(c_{dt_M} + c_{pi_M})x_1 - k_{pi_M}x_2 + c_{pi_M}x_3] \\ &+ \lambda(x_1 - x_d) + \lambda(x_1 - x_7) \end{aligned} \tag{38}$$

Since $\Gamma(x(t))$ is a positive constant equal $1/J_{dt}$, Γ_m can be replaced with $1/J_{dt}$ and this could not affect the convergence proof. Substituting Equation (37) into Equation (19) gives the following:

$$\begin{aligned} \dot{V(t)} \leq &\mid s \mid \psi_{ma} - \mid s \mid (1/J_{dt})\hat{k_1}(t) \mid s \mid^{1/2} - a(1/J_{dt})\hat{k_1}(t) \mid s \mid^2 \\ &+ \frac{1}{\gamma}(\hat{k_1}(t) - \bar{k_1})\mu_1 \mid s \mid^b sign(\mid s \mid - \delta) \end{aligned} \tag{39}$$

Adding and substituting the term $1/J_{dt}\bar{k_1}(|s|^{1/2} - a|s|)$ gives the following:

$$\begin{aligned} \dot{V(t)} \leq &\mid s \mid \psi_{ma} - \mid s \mid (1/J_{dt})\hat{k_1}(t)(\mid s \mid^{1/2} - a \mid s \mid) \\ &+ \frac{1}{\gamma}(\hat{k_1}(t) - \bar{k_1})\mu_1 \mid s \mid^b sign(\mid s \mid - \delta) \\ &+ \mid s \mid (1/J_{dt})\bar{k_1}(\mid s \mid^{1/2} - a \mid s \mid) - \mid s \mid (1/J_{dt})\bar{k_1}(\mid s \mid^{1/2} - a \mid s \mid) \end{aligned} \tag{40}$$

After simplification, this gives the following:

$$\begin{aligned} \dot{V(t)} \leq &\mid s \mid [\psi_{ma} - (1/J_{dt})\bar{k_1}(\mid s \mid^{1/2} - a \mid s \mid)] \\ &+ (\hat{k_1}(t) - \bar{k_1})[- \mid s \mid (1/J_{dt})\hat{k_1}(t)(\mid s \mid^{1/2} - a \mid s \mid) \\ &+ \frac{1}{\gamma}\mu_1 \mid s \mid^b sign(\mid s \mid - \delta)] \end{aligned} \tag{41}$$

Let us define a positive constant β; in this case:

$$\begin{aligned} \dot{V(t)} \leq &\mid s \mid [\psi_{ma} - (1/J_{dt})\bar{k_1}(\mid s \mid^{1/2} - a \mid s \mid)] \\ &+ (\hat{k_1}(t) - \bar{k_1})[- \mid s \mid (1/J_{dt})\hat{k_1}(t)(\mid s \mid^{1/2} - a \mid s \mid) \\ &+ \frac{1}{\gamma}\mu_1 \mid s \mid^b sign(\mid s \mid - \delta)] + \beta \mid \hat{k_1}(t) - \bar{k_1} \mid - \beta \mid \hat{k_1}(t) - \bar{k_1} \mid \end{aligned} \tag{42}$$

Therefore,

$$\begin{aligned} \dot{V(t)} \leq & - \mid s \mid (-\psi_{ma} + (1/J_{dt})\bar{k_1}(\mid s \mid^{1/2} - a \mid s \mid)) \\ & - \beta \mid \hat{k_1}(t) - \bar{k_1} \mid - \mid \hat{k_1}(t) - \bar{k_1} \mid s \mid^{3/2} ((1/J_{dt})\hat{k_1}(t)(1 - a \mid s \mid^{1/2})) \\ & - \mid \hat{k_1}(t) - \bar{k_1} \mid (\frac{1}{\gamma}\mu_1 \mid s \mid^{b} sign(\mid s \mid -\delta) + \beta) \end{aligned} \tag{43}$$

If we consider these two assumptions, then the time derivative of $V(t)$, denoted as $\dot{V}(t)$, will be negative.

$$\begin{aligned} 1 - a|s|^{1/2} > 0 \\ -\frac{1}{\gamma}\mu_1 sign(|s| - \delta) + \beta > 0 \end{aligned} \tag{44}$$

Therefore, following the same steps as the general convergence section, the closed-loop convergence can be proved. The equivalent control is defined as the solution of $\dot{s} = 0$, which can be expressed as follows:

$$u_{eq} = c_{pi}(x_1 - x_3) + k_{pi}x_2 + c_{dt}x_1 - J_{dt}\lambda(x_1 - x_d) - J_{dt}\lambda(x_1 - x_7) \tag{45}$$

In Equation (30), the sliding surface depends on the velocities of both the drill bit and the rotary table following a desired reference velocity. Generally, the drill string can be driven with various reference velocities depending on the length and diameter of the drill string and the type of rock of the borehole. These velocities are chosen in order to have an adequate rate of penetration, providing fast drilling while maintaining the integrity of the drilling components. All variables existing in the control command are supposed to be bounded as follows:

$$\begin{cases} x_1 \in [x_{1min}, x_{1max}]RPM \\ x_7 \in [x_{7min}, x_{7max}]RPM \end{cases}$$

The desired velocity x_d is bounded as well. This implies that both u_{eq} and u_{disc} are limited signals, which ensures that the control input u is a bounded signal with the following:

$$u \in [u_{min}, u_{max}]kN.m \tag{46}$$

4. Validation and Results

To evaluate the effectiveness of the suggested control approach, simulations were carried out using a drill string system. The aim of the controller was to follow a desired reference velocity and to counteract external disturbances in various operational conditions and with varying parametric uncertainties. The proposed controller (Proposed) was compared with various other controllers, including classic first-order SMC (CSMC), modified first-order SMC (MSMC), and the well-known adaptive SMC (ASMC). The switching law of CSMC, as described in [34], is as follows:

$$\mu_{sw1} = -k_1 sign(s) \tag{47}$$

According to [21], the MSMC is described as an exponent reaching law as follows:

$$\mu_{sw2} = -k_2|s|^{1/2}sign(s) - k_3 s \tag{48}$$

The well-known adaptive controller proposed in [38] is described by the following switching law and gain dynamics:

$$\mu_{disc} = -\hat{k_4}(t)sign(s) \tag{49}$$

where the dynamics of the controller gain are as follows:

$$\dot{\hat{k}}_4(t) = \begin{cases} \mu_{11}|s|sign(|s| - \delta_2) & \text{if } \hat{k}_4(t) > \mu_{22} \\ \mu_{22} & \text{if } \hat{k}_4(t) \leq \mu_{22} \end{cases} \tag{50}$$

where k_1 is large enough to counteract the external perturbations, k_2 and k_3 are positive constants, and $u_{11} > 0$ and $u_{22} > 0$ are very small. Table 1 gives the different parameter values for each controller with optimal adjustments.

Table 1. Parameter adjustments for each controller.

Controller	Parameters	Value
CSMC	k_1	3
SMCm	k_2	3
	k_3	0.001
ASMC	μ_{11}	0.1
	μ_{22}	0.01
Proposed	μ_1	3
	μ_2	0.001
	α	0.1
	a	0.01
	b	0.125

The values of the parameters were selected to achieve optimal performance while maintaining a balance between the overshoot and settling time of the controllers, based on a given reference velocity and WOB.

4.1. Performance Criteria

To assess the performance of the various controllers, several performance metrics were used. The first measure was the integral square error (ISE), which evaluates the energy associated with the error by integrating the square of the error over time, and it emphasizes large errors. The ISE can be expressed as follows:

$$ISE = \int e^2 dt \tag{51}$$

where:

$$e = V_{ref} - V_{bit} \tag{52}$$

The integral absolute error (IAE) measures the integral of the absolute error over time and provides an idea of the cumulative errors. It is useful for evaluating the performance of a controller in terms of the overall deviation from the desired trajectory. The IAE can be defined as follows:

$$IAE = \int |e| dt \tag{53}$$

In order to evaluate the steady-state error, the root mean square error (RMSE) was employed by calculating the square root of the average of squared errors over a specified time period, the RMSE provides an effective measure of the discrepancy between desired and actual values, taking into account the entire sample set. This metric assumes a Gaussian distribution of errors and is widely adopted as a reliable method for quantifying the accuracy of a system's response.

$$RMSE = \sqrt{\int \frac{e^2}{n} dt} \tag{54}$$

where n is the number of samples over time. The energy consumption of each controller can be quantified by the root mean square deviation (RMSD), which is defined as follows:

$$RMSD = \sqrt{\int \frac{T^2}{n} dt} \tag{55}$$

where T is the torque input of the drive table. This criterion is very important since a controller with minimal energy consumption is greatly desired in order to save money in terms of energy, maintenance, etc. Overshoot (O%) and settling time (ST) criteria were also used to evaluate the controllers. These are calculated as follows:

$$O\% = \frac{peak\ value - final\ value}{final\ value} \times 100\% \tag{56}$$

The variable "ST" signifies the time required to achieve and sustain stability within a defined range, typically set at 5% of the final value. This measure captures the duration it takes for the system's response to settle and remain within an acceptable margin of variation.

4.2. Simulation Results

Multiple experiments were performed using the MATLAB/Simulink platform, employing a sampling frequency of $fs = 1$ kHz. These tests aimed to evaluate the resilience of each controller when subjected to diverse operating conditions, including measurement noise and parametric uncertainties related to the stiffness and damping of the drill pipes, as well as the damping of the drive table. The selected parameters listed in Table 2 were extracted from an actual drill string system documented in [19]. These parameters were chosen based on their relevance and applicability to the specific drill string system under investigation.

Table 2. Numerical values for the simulation parameters.

Parameter	Symbol	Value	Units
Moment of inertia of the drive table	J_{dt}	930	kg·m^2
Moment of inertia of the drill bit	J_{bi}	471.96	kg·m^2
Moment of inertia of the drill pipes	J_{pi}	2782.25	kg·m^2
Moment of inertia of the drill collar	J_{co}	750	kg·m^2
Torsional damping between drive table and drill pipe	C_{dt}	425	N·m·s/rad
Torsional damping between the drill pipe and BHA	C_{bit}	50	N·m·s/rad
Torsional damping between BHA and drill bit	C_{co}	190	N·m·s/rad
Torsional damping between BHA and drill pipe	C_{pi}	193.61	N·m·s/rad
Torsional stiffness between drive table and drill pipe	k_{pi}	698.06	N·m/rad
Torsional stiffness between drill collar and BHA	k_{co}	1080	N·m/rad
Torsional stiffness between BHA and drill bit	k_{bi}	907.48	N·m/rad
Decline rate of friction torque	ξ	0.5	s/rad
Static and sliding friction threshold	Δw	0.001	rad/s
Radius of the drill bit	R	0.15	m
Coulomb friction coefficient	μ_a	0.8	—
Static friction coefficient	μ_0	0.5	—

In the remainder of the paper, the results of the various tests mentioned above will be presented alongside an analysis of the results obtained via the evaluation criteria already defined (Equations (50)–(55)).

4.2.1. Robustness to Measurement Noise

The robustness of the measurement noise section was tested to approximate experimental tests as closely as possible. Various sources can be implemented to represent noise. They all share the ability to add random variation to the signal under study. In the

simulation studies, random white noise was selected as the noise source. This type of noise has a stochastic nature and is characterized by having equal power across all frequencies, making it suitable for imitating measurement noise [26]. By studying the behavior of controllers under such conditions, we can gain valuable insights into their robustness and adaptability. The system under control was subjected to a controlled level of white noise with a noise amplitude of 10^{-4} dB. The bit velocities of the controllers were then analyzed, and the outcomes were recorded in Figure 3. As shown in Figure 4a,b, the proposed controller exhibited the least response to measurement noise. Quantitative measurements revealed that the proposed controller achieved an average chattering magnitude reduction of 20% compared to the CSMC, 14% compared to the MSMC, and 18% compared to the ASMC. These numbers highlight the substantial advantage of the proposed controller in mitigating chattering.

The proposed controller showed a remarkable reduction in chattering magnitude compared to the other controllers while consuming the least energy. This proves that the proposed controller was the least affected by measurement noise. In addition to its success in chattering reduction, the proposed adaptive methodology has also demonstrated superior performance in terms of energy consumption compared to a previously proposed adaptive sliding mode controller [26]. Figure 5 shows the RMSD values of the proposed controller versus CSMS, MSMC, and ASMC controllers. The developed controller in [26] exhibited an RMSD value of 13,016, indicating a higher level of energy consumption. However, with the introduction of the new proposed controller, an improvement has been achieved, resulting in a smaller RMSD value of 13,012. The reduction signifies a noteworthy enhancement in energy efficiency. The reduction is due to the $|s|^b$ term in the proposed gain dynamics, which presents the key parameter that helped decrease the chattering effect. This improvement indicates that the proposed adaptive methodology optimizes the energy consumption of the system, resulting in reduced waste and increased overall energy efficiency.

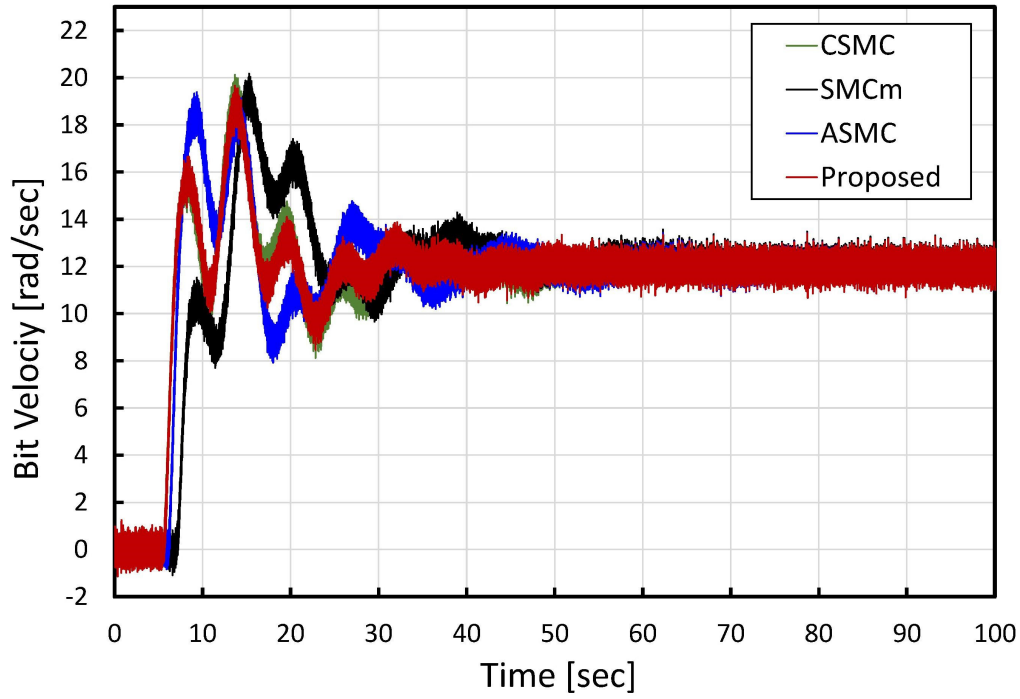
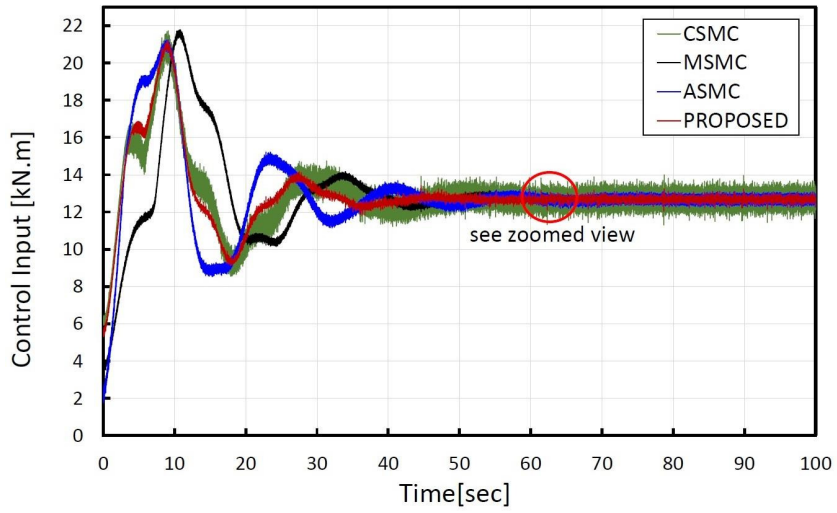
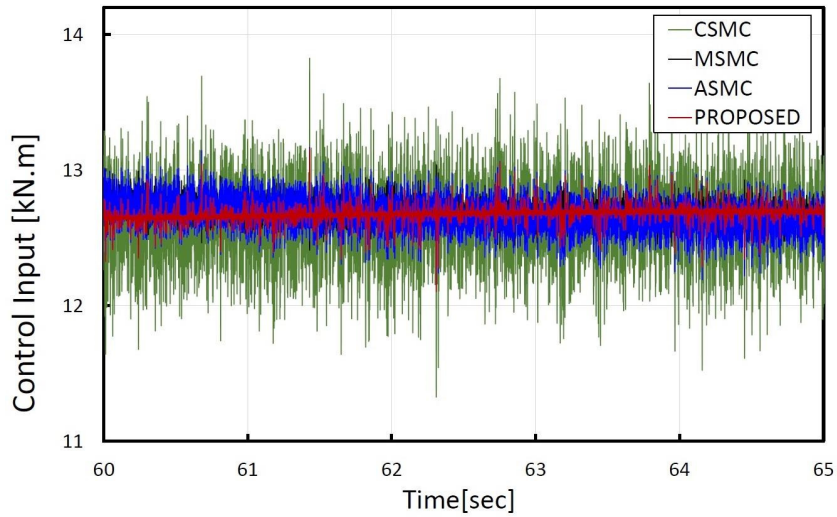


Figure 3. Effects of measurement noise on drill string bit velocities.



(**a**)



(**b**)

Figure 4. Effects of measurement noise on input signals; (**a**) global scale; and (**b**) local scale.

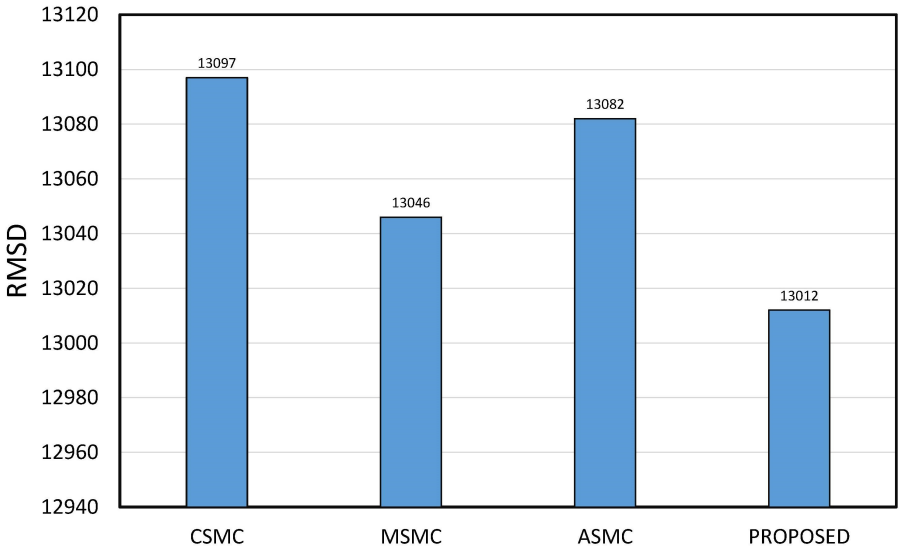


Figure 5. RMSD values of different controllers.

4.2.2. Robustness to Parametric Uncertainties

In the literature, different stochastic and deterministic approaches have been applied to drill strings to investigate the problem of uncertainties. The research in [39,40] presented some examples of stochastic models. The authors in [41] proposed a stochastic model for the bit-rock interaction torque. This was achieved by introducing uncertain parameters into the dry friction model and subsequently conducting a Monte Carlo simulation. Adaptive techniques for the deterministic approach were also explored, such as the direct adaptive controller proposed in [42], which proved to be robust against changes in friction characteristics and induced noise. It is worth mentioning that the convergence of the controller can be affected by an inappropriate setup of the adaptive algorithms. In the subsequent simulations, parametric uncertainties were introduced for the drill pipes' stiffness and damping, as well as the drive table's damping. According to Equation (35), the equivalent control incorporating parametric uncertainties can be expressed as follows:

$$\begin{aligned} u_{eq} = \quad & \Delta_1 c_{pi}(x_1 - x_3) + \Delta_2 k_{pi} x_2 + \Delta_3 c_{dt} x_1 \\ & - J_{dt}\lambda(x_1 - x_d) - J_{dt}\lambda(x_1 - x_7) \end{aligned} \tag{57}$$

To evaluate the performance of various controllers under diverse operating conditions, an investigation was conducted to analyze the influence of different parametric uncertainties on the system's performance. The purpose here is to gain insights into the controllers' effectiveness and assess their robustness in handling varying parametric uncertainties. These uncertainties are categorized into three conditions: condition 1, condition 2, and condition 3. Condition 1 refers to small parametric uncertainties, where the variations in the parameters are relatively minor. Condition 2 corresponds to medium parametric uncertainties, where the variations in the parameters are of moderate magnitude. Finally, condition 3 represents large parametric uncertainties, characterized by significant variations in the parameters. By examining the system's behavior under these distinct conditions, we aim to assess its robustness and performance across a range of parametric uncertainties, as shown in Table 3.

Table 3. Conditions of parametric uncertainties.

Parametric Uncertainties	Δ_1 (%)	Δ_2 (%)	Δ_3 (%)
Nominal condition	0	0	0
Condition 1	40	30	30
Condition 2	60	50	40
Condition 3	75	75	75

To clearly demonstrate the responses of each controller to different variations, separate figures were used. Figure 6 depicts that the CSMC remained robust for small parametric uncertainties. However, when subjected to medium parametric uncertainties, the system exhibited convergence but with a significant static error of 4 rad/s from the desired reference velocity. In addition, the system lost its robustness and experienced the stick–slip phenomenon for large parametric uncertainties. In Condition 1, the controller was robust with a smaller overshoot value, and no parametric adjustment was required. However, for Conditions 2 and 3, the responses became mediocre and asymptotically stable, respectively. The controller's parameters need to be adjusted in these cases.

Figure 7 demonstrates that the system response diverges completely, independently from the magnitudes of the parametric uncertainties. Therefore, it can be concluded that the MSMC is not robust even to minimal parametric uncertainties. In order to ensure stability and acceptable performance in the presence of any parametric variation, parametric adjustment is necessary.

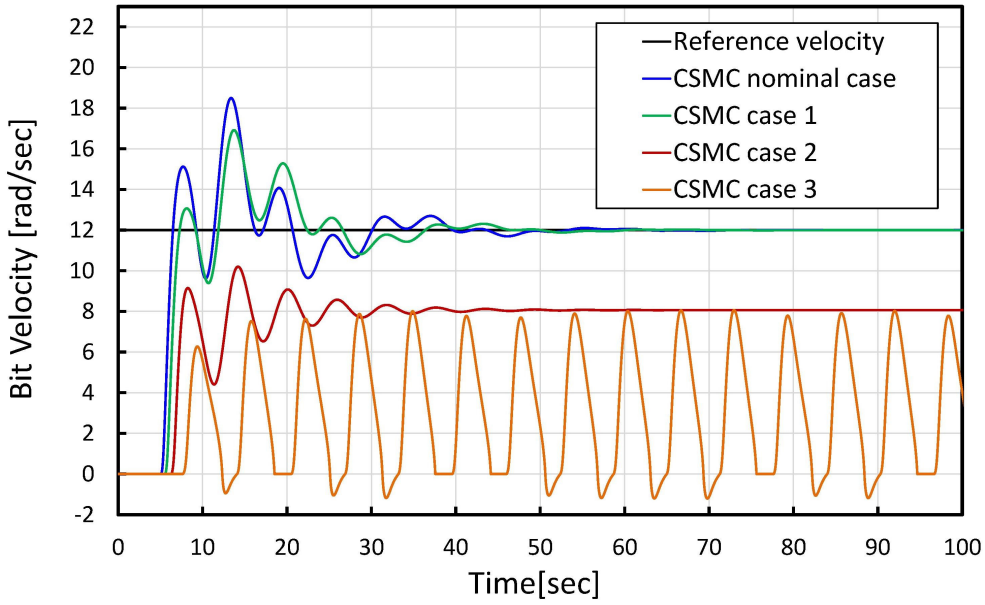


Figure 6. System responses of the CSMC with parametric uncertainty.

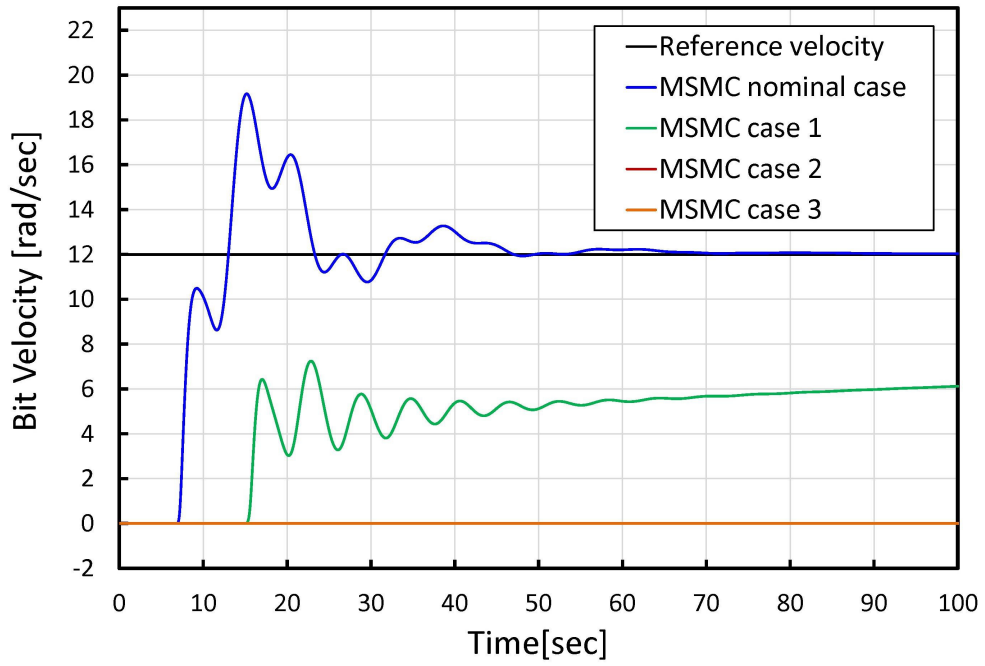


Figure 7. System responses of the MSMC with parametric uncertainty.

For all cases of parametric uncertainty, the ASMC system's trajectory converged to the reference velocity (see Figure 8). It should be noted that the settling time of the system response increases considerably by nearly 20% for large parametric uncertainties.

Figure 9 shows that the proposed controller maintains its robustness regardless of variation in the parameters. This proves that the proposed controller does not need any parameter adjustments for any of the cases of parametric uncertainty, which demonstrates the fast adaptability of the gains.

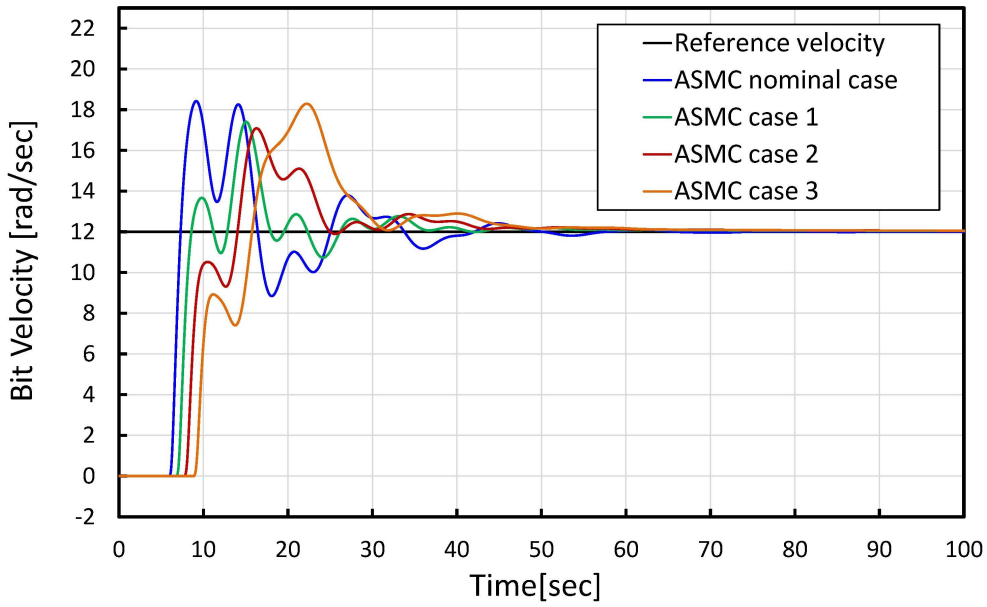


Figure 8. System responses of the ASMC with parametric uncertainty.

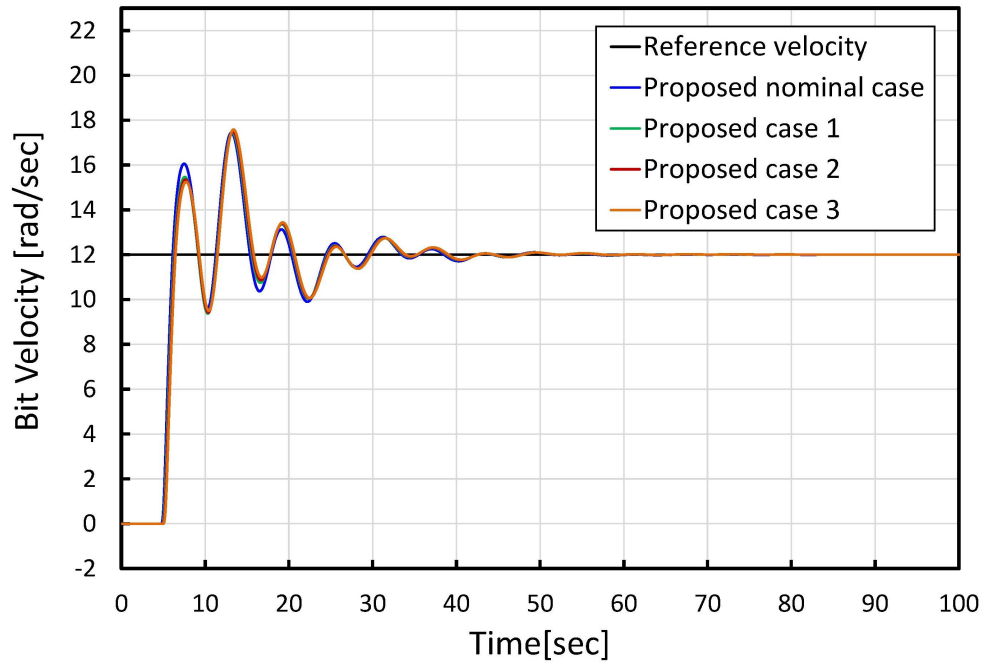


Figure 9. System responses of the proposed controller with parametric uncertainty.

Figures 10–12 show that the proposed controller had the smallest integral square error whereas the MSMC had the greatest value, with a difference of 35%. This indicates that the proposed algorithm had the least amount of error energy, while the MSMC had the highest amount of errors. The proposed algorithm had a smaller IAE value than the MSMC controller by almost 20%, indicating a closer response to the reference velocity. The RMSD values were used to compare the energy consumption of the different controllers, both with and without added measurement noise. As can be seen, the maximum energy consumption was found for the ASMC, whereas the minimum was found for the proposed controller. This criterion is very important since it affects the lifetime of the component. The proposed controller had the smallest RMSE value, which proves that it had the least steady-state error. This shows the good precision of the regulator and results in good static performance, which is required for such an application.

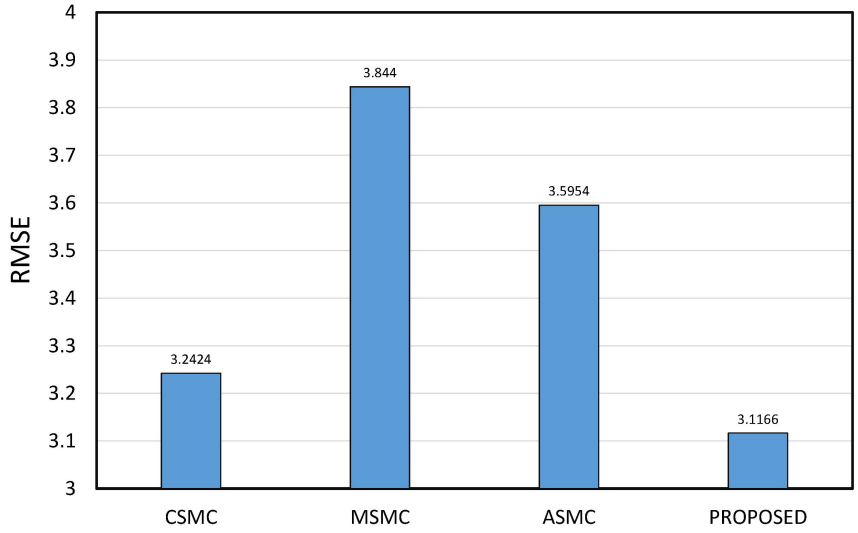


Figure 10. Root mean square error (RMSE) of different controllers.

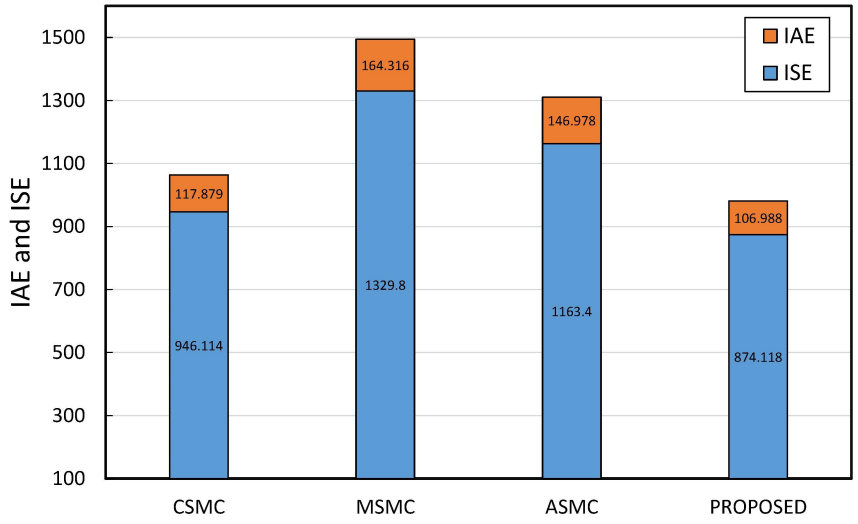


Figure 11. The ISE (integral square error) and IAE (integral absolute error) values for all controllers.

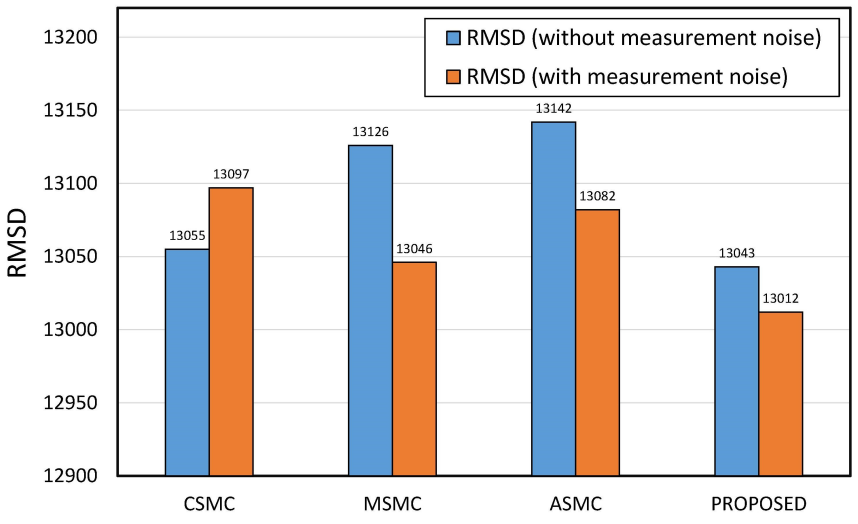


Figure 12. RMSD values with and without measurement noise for all controllers.

Table 4 presents a summary of the results comparing four controllers based on several performance metrics. The metrics considered are EC (energy consumption), RPU (robustness to parametric uncertainty), RMN (robustness to measurement noise), and P (static precision). These metrics provide insights into the controllers' energy efficiency, their ability to handle uncertainties in system parameters and measurement noise, and their resilience to variations in weight on bit and reference velocity. The table offers a comprehensive evaluation of the controllers, facilitating a thorough assessment of their performance in different operational aspects. The controller with the best performance for each category is indicated by the "High" or "Very High" rating, while the worst performance is indicated by the "Low" rating. Table 4 shows that the proposed controller performed better in terms of precision, convergence time, and overshoot compared with both classical and adaptive SMCs. Given its robustness to parametric uncertainty and measurement noise, the proposed controller guaranteed minimal chattering, resulting in a smooth input signal. It is worth mentioning that a previous article presented an adaptive controller that yielded favorable results [43]. However, it is important to note that this controller did not undergo tests specifically examining its performance in the presence of measurement noise.

Table 4. Comparative analysis of controllers based on performance metrics.

Controller	EC	RPU	RMN	P
CSMC	High	Low	Low	High
MSMC	Low	Low	Low	Low
ASMC	Low	High	High	High
Presented in [43]	Unknown	Very High	Unknown	Very High
Proposed	Very High	Very High	Very High	Very High

5. Conclusions

In summary, this paper presents a novel adaptive sliding mode control (SMC) approach aimed at suppressing stick–slip vibrations in drilling string systems. A new switching adaptive SM controller based on an exponent reaching law is introduced, which dynamically updates controller gains in real time. Through comprehensive simulations and analysis, the effectiveness of the proposed control strategy in improving drilling string performance while minimizing stick–slip phenomena is demonstrated. The proposed controller offers several advantages over traditional control methods, including robustness to measurement noise, resilience to parametric uncertainties, and convergence in finite time without requiring prior knowledge of uncertainties or disturbances. By adjusting the controller gains in real-time and using dynamic adjustments, the adaptive SMC approach achieves superior performance in suppressing stick–slip vibrations compared to conventional SMC techniques. Furthermore, to help other researchers effectively address the stick–slip phenomenon in drill string systems, the following engineering suggestions are recommended:

- Select appropriate modeling approach: choose the most suitable modeling approach based on the specific requirements of the drilling operation. Torsional models are particularly effective for addressing stick–slip vibrations, while coupled models are better suited for mitigating bit bounce or whirling phenomena.
- Consider certain assumptions for drill string modeling: this includes considering stiffness and damping factors and the relationship between weight on bit (WOB) and torque on bit to refine the modeling approach.
- Account for nonlinear effects in torque on bit calculations: account for nonlinear effects by choosing adequate models such as the Karnopp friction model. Understanding and accounting for these nonlinearities are crucial for developing robust control strategies.
- Prioritize the integration of adaptive robust control strategies into drill string systems: such control mechanisms can enhance system robustness and performance by dynamically adjusting to varying operating conditions and disturbances.

Author Contributions: Conceptualization, M.G. and L.S.; methodology, F.Z. and L.S.; software, F.Z.; validation, F.Z.; formal analysis, F.Z. and L.S.; investigation, F.Z. and L.S.; resources, M.G.; data curation, M.G.; writing—original draft preparation, F.Z.; writing—review and editing, F.Z. and M.G.; visualization, M.G.; supervision, M.G.; project administration, M.G.; funding acquisition, M.G. All authors have read and agreed to the published version of the manuscript.

Funding: This research was funded by Qatar National Research Fund grant number NPRP10-0101-170081.

Institutional Review Board Statement: Not applicable.

Informed Consent Statement: Not applicable.

Data Availability Statement: The data presented in this study are available upon request from the corresponding author.

Acknowledgments: This publication was made possible by NPRP grant [NPRP10-0101-170081] from the Qatar National Research Fund (a member of Qatar Foundation).

Conflicts of Interest: The authors declare no conflicts of interest.

Abbreviations

The following abbreviations are used in this manuscript:

Acronym	**Definition**
ASMC	Adaptive Sliding Mode Controller
CPDE	Coupled Partial Differential Equation
CSMC	Classic Sliding Mode Controller
DOF	Degrees Of Freedom
LQG	Linear–Quadratic–Gaussian
ODEs	Ordinary Differential Equations
PD	Proportional–Derivative
PI	Proportional–Integral
PID	Proportional–Integral–Derivative
ROP	Rate Of Penetration
SM	Sliding Mode
SMC	Sliding Mode Controller
SMCm	Modified Sliding Mode Controller
WOB	Weight On Bit

Symbol	**Parameter**
s	Sliding surface
$\Re$, ψ, Γ	Uncertain functions belonging to the set
u	Control input
λ	Positive constant
$\dot{s}$	The time derivative of the sliding surface
V	The candidate Lyapunov function
δ, u_1, u_2, a	Positive constants
$\bar{k_1}$	Adaptive gain upper bound
k_1, k_2, k_3	Positive gains
$\hat{k_4}$	Adaptive gain of ASMC
V_{ref}	Required reference velocity
V_{bit}	Bit velocity
Δ_2, $u_1 1$, $u_2 2$	Positive constants

References

1. Taleb, M.; Plestan, F.; Bououlid, B. Higher order sliding mode control based on adaptive first order sliding mode controller. *IFAC Proc. Vol.* **2014**, *47*, 1380–1385. [CrossRef]
2. Sira-Ramirez, H. On the dynamical sliding mode control of nonlinear systems. *Int. J. Control* **1993**, *57*, 1039–1061. [CrossRef]
3. Shao, K.; Zheng, J.; Wang, H.; Xu, F.; Wang, X.; Liang, B. Recursive sliding mode control with adaptive disturbance observer for a linear motor positioner. *Mech. Syst. Signal Process.* **2021**, *146*, 107014. [CrossRef]

4. Li, H.; Maghareh, A.; Montoya, H.; Uribe, J.W.C.; Dyke, S.J.; Xu, Z. Sliding mode control design for the benchmark problem in real-time hybrid simulation. *Mech. Syst. Signal Process.* **2021**, *151*, 107364. [CrossRef]
5. Tan, S.C.; Lai, Y.; Tse, C.K.; Cheung, M.K. Adaptive feedforward and feedback control schemes for sliding mode controlled power converters. *IEEE Trans. Power Electron.* **2006**, *21*, 182–192.
6. Liu, X.; Su, X.; Shi, P.; Shen, C.; Peng, Y. Event-triggered sliding mode control of nonlinear dynamic systems. *Automatica* **2020**, *112*, 108738. [CrossRef]
7. Zou, M.; Fang, P.; Hou, Y.; Wang, Y.; Hou, D.; Peng, H. Synchronization analysis of two eccentric rotors with double-frequency excitation considering sliding mode control. *Commun. Nonlinear Sci. Numer. Simul.* **2021**, *92*, 105458. [CrossRef]
8. Zhang, Y.; Shi, Z. Sliding mode control for uncertain TS fuzzy singular biological economic system. *IEEE Access* **2019**, *7*, 14387–14395. [CrossRef]
9. Tian, B.; Cui, J.; Lu, H.; Zong, Q. Reentry attitude control for RLV based on adaptive event-triggered sliding mode. *IEEE Access* **2019**, *7*, 68429–68435. [CrossRef]
10. Ahmed, S.; Ahmed, A.; Mansoor, I.; Junejo, F.; Saeed, A. Output feedback adaptive fractional-order super-twisting sliding mode control of robotic manipulator. *Iran. J. Sci. Technol. Trans. Electr. Eng.* **2021**, *45*, 335–347. [CrossRef]
11. Nobahar Sadeghi, A.; Arıkan, K.B.; Özbek, M.E.; Baranoğlu, B. Robust and adaptive control design of a drilling rig during the operating modes. *Meas. Control* **2019**, *52*, 702–719. [CrossRef]
12. Sadeghimehr, R.; Nikoofard, A.; Khaki Sedigh, A. Predictive-based sliding mode control for mitigating torsional vibration of drill string in the presence of input delay and external disturbance. *J. Vib. Control* **2020**, *27*, 2432–2450. [CrossRef]
13. Ahamed, N.U.; Yusof, Z.; Hamedon, Z.; Rabbi, M.F.; Sikandar, T.; Palaniappan, R.; Ali, M.A.; Rahman, S.M.; Sundaraj, K. Fuzzy logic controller design for intelligent drilling system. In Proceedings of the 2016 IEEE International Conference on Automatic Control and Intelligent Systems (I2CACIS), Selangor, Malaysia, 22 October 2016; pp. 208–213.
14. Raviraj, V.; Sen, P.C. Comparative study of proportional-integral, sliding mode, and fuzzy logic controllers for power converters. *IEEE Trans. Ind. Appl.* **1997**, *33*, 518–524. [CrossRef]
15. Capisani, L.M.; Ferrara, A.; Magnani, L. Design and experimental validation of a second-order sliding-mode motion controller for robot manipulators. *Int. J. Control* **2009**, *82*, 365–377. [CrossRef]
16. Derafa, L.; Fridman, L.; Benallegue, A.; Ouldali, A. Super twisting control algorithm for the four rotors helicopter attitude tracking problem. In Proceedings of the 2010 11th International Workshop on Variable Structure Systems (VSS), Mexico City, Mexico, 26–28 June 2010; pp. 62–67.
17. Fei, J.; Feng, Z. Fractional-order finite-time super-twisting sliding mode control of micro gyroscope based on double-loop fuzzy neural network. *IEEE Trans. Syst. Man Cybern. Syst.* **2020**, *51*, 7692–7706. [CrossRef]
18. Fei, J.; Chen, Y. Fuzzy double hidden layer recurrent neural terminal sliding mode control of single-phase active power filter. *IEEE Trans. Fuzzy Syst.* **2020**, *29*, 3067–3081. [CrossRef]
19. Fei, J.; Wang, H. Experimental investigation of recurrent neural network fractional-order sliding mode control of active power filter. *IEEE Trans. Circuits Syst. II Express Briefs* **2019**, *67*, 2522–2526. [CrossRef]
20. Rodriguez, J.; Castañeda, H.; Gordillo, J. Design of an Adaptive Sliding Mode Control for a Micro-AUV Subject to Water Currents and Parametric Uncertainties. *J. Mar. Sci. Eng.* **2019**, *7*, 445. [CrossRef]
21. Castañeda, H.; Gordillo, J.L. Embedded Flight Control Based on Adaptive Sliding Mode Strategy for a Quadrotor Micro Air Vehicle. *Electronics* **2019**, *8*, 793. [CrossRef]
22. Fei, J.; Chen, Y. Dynamic terminal sliding-mode control for single-phase active power filter using new feedback recurrent neural network. *IEEE Trans. Power Electron.* **2020**, *35*, 9904–9922. [CrossRef]
23. Huang, Y.J.; Kuo, T.C.; Chang, S.H. Adaptive sliding-mode control for nonlinearsystems with uncertain parameters. *IEEE Trans. Syst. Man, Cybern. Part B (Cybern.)* **2008**, *38*, 534–539. [CrossRef]
24. Li, P.; Zheng, Z.Q. Robust adaptive second-order sliding-mode control with fast transient performance. *IET Control Theory Appl.* **2012**, *6*, 305–312. [CrossRef]
25. Edwards, C.; Shtessel, Y.B. Adaptive continuous higher order sliding mode control. *Automatica* **2016**, *65*, 183–190. [CrossRef]
26. Zribi, F.; Sidhom, L.; Gharib, M.; Refaat, S.S. New algorithm based active method to eliminate stick-slip vibrations in drill string systems. *Syst. Sci. Control Eng.* **2022**, *10*, 468–487. [CrossRef]
27. Cheng, J.; Wu, M.; Wu, F.; Lu, C.; Chen, X.; Cao, W. Modeling and Control of Drill-String System with Stick-Slip Vibrations Using LPV Technique. *IEEE Trans. Control. Syst. Technol.* **2020**, *29*, 718–730. [CrossRef]
28. Dao, N.H.; Menand, S.; Isbell, M. Mitigating and understanding stick-slip in unconventional wells. In Proceedings of the SPE/IADC International Drilling Conference and Exhibition, The Hague, The Netherlands, 5–7 March 2019; p. SPE-194117-MS.
29. Yang, L.; Tian, J.; Liu, Q.; Dai, L.; Hu, Z.; Li, J. The multidirectional vibration and coupling dynamics of drill string and its influence on the wellbore trajectory. *J. Mech. Sci. Technol.* **2020**, *34*, 2681–2692. [CrossRef]
30. Jansen, J.D.; Van Den Steen, L. Active damping of self-excited torsional vibrations in oil well drillstrings. *J. Sound Vib.* **1995**, *179*, 647–668. [CrossRef]
31. Dunayevsky, V.; Abbassian, F. Application of stability approach to bit dynamics. *SPE Drill. Complet.* **1998**, *13*, 99–107.
32. Navarro-López, E.M.; Suárez, R. Practical approach to modelling and controlling stick-slip oscillations in oilwell drillstrings. In Proceedings of the 2004 IEEE International Conference on Control Applications, Taipei, Taiwan, 2–4 September 2004; Volume 2, pp. 1454–1460.

33. Puebla, H.; Alvarez-Ramirez, J. Suppression of stick-slip in drillstrings: A control approach based on modeling error compensation. *J. Sound Vib.* **2008**, *310*, 881–901. [CrossRef]
34. Navarro-López, E.M.; Licéaga-Castro, E. Non-desired transitions and sliding-mode control of a multi-DOF mechanical system with stick-slip oscillations. *Chaos Solitons Fractals* **2009**, *41*, 2035–2044. [CrossRef]
35. Abdulgalil, F.; Siguerdidjane, H. Backstepping design for controlling rotary drilling system. In Proceedings of the 2005 IEEE Conference on Control Applications, Toronto, ON, Canada, 28–31 August 2005; pp. 120–124.
36. Fu, M.; Zhang, P.; Li, J.; Wu, Y. Observer and reference governor based control strategy to suppress stick-slip vibrations in oil well drill-string. *J. Sound Vib.* **2019**, *457*, 37–50. [CrossRef]
37. Liu, Y. Control of a class of multibody underactuated mechanical systems with discontinuous friction using sliding-mode. *Trans. Inst. Meas. Control* **2018**, *40*, 514–527. [CrossRef]
38. Plestan, F.; Shtessel, Y.; Bregeault, V.; Poznyak, A. New methodologies for adaptive sliding mode control. *Int. J. Control* **2010**, *83*, 1907–1919. [CrossRef]
39. Lobo, D.; Ritto, T.; Castello, D. A novel stochastic process to model the variation of rock strength in bit-rock interaction for the analysis of drill-string vibration. *Mech. Syst. Signal Process.* **2020**, *141*, 106451. [CrossRef]
40. Chen, J.; Liao, H.; Zhang, Y.; Liang, H.; Liu, C.; Qi, D. A torsional-axial vibration analysis of drill string endowed with kinematic coupling and stochastic approach. *J. Pet. Sci. Eng.* **2021**, *198*, 108157. [CrossRef]
41. Trindade, M.A. Robust evaluation of stability regions of oil-well drilling systems with uncertain bit-rock nonlinear interaction. *J. Sound Vib.* **2020**, *483*, 115481. [CrossRef]
42. Wasilewski, M.; Pisarski, D.; Konowrocki, R.; Bajer, C.I. A new efficient adaptive control of torsional vibrations induced by switched nonlinear disturbances. *Int. J. Appl. Math. Comput. Sci.* **2019**, *29*, 285–303. [CrossRef]
43. Zribi, F.; Sidhom, L.; Krama, A.; Gharib, M. Enhancement of drill string system operations with adaptive robust controller and hardware in-the-loop validation. *J. Sound Vib.* **2023**, *556*, 117716. [CrossRef]

Disclaimer/Publisher's Note: The statements, opinions and data contained in all publications are solely those of the individual author(s) and contributor(s) and not of MDPI and/or the editor(s). MDPI and/or the editor(s) disclaim responsibility for any injury to people or property resulting from any ideas, methods, instructions or products referred to in the content.